JOURNAL OF MATERIALS SCIENCE **36** (2001) 7–20

Effect of rubber interlayers on the fracture of glass bead/epoxy composites

JONGHWI LEE*, ALBERT F. YEE‡
Macromolecular Science and Engineering Program, The University of Michigan, Ann Arbor, MI 48109, USA
E-mail: afyee@engin.umich.edu

The effectiveness of rubber interlayers between inorganic particles and polymer matrix for toughening has been a controversial subject. In this research, a series of rubber-encapsulated glass beads and its epoxy composites were prepared, and underlying mechanisms which can connect material parameters related with rubber interlayers with energy dissipation mechanisms, were investigated. The critical stress intensity factor (K_{IC}) and critical strain energy release rate (G_{IC}) of rubber-encapsulated glass bead filled epoxies were found to insignificantly depend on the existence and thickness of rubber interlayers. Microscopy studies on fracture process identified four different micro-mechanical deformations which can dissipate fracture energy: step formation, micro-shear banding, debonding of glass beads, and diffuse matrix shear yielding. It was found that the first two became less extensive and the others became more extensive as the thickness of rubber interlayers increases. This offsetting effect of micro-mechanical deformations seems to be the reason for the absence of significant toughening effect of rubber interlayers.

1. Introduction

It is well known that most polymers can be made tougher by the addition of a small amount of rubbery particles, dispersed on a microscopic scale [1, 2]. But this toughening is achieved with a loss in modulus and hardness of the material. On the other hand, inorganic particles such as silica, alumina and talc can improve both toughness and modulus [1–3]. Unfortunately, this toughness increase by inorganic particles is usually smaller than that achievable by rubbery particles. Thus, it has been suggested that combinations of inorganic particles and rubber may be able to give effective toughening without loss in modulus and strength [4]. Simple hybrid-particulate composites with separate dispersions of inorganic and rubber particles have been studied by several research groups [5–7]. Their studies show that it is possible for this simple combination to toughen as well as stiffen polymer matrices.

Core/shell structures of inorganic particles encapsulated by rubber, has been developed to improve the effectiveness of the rubber and the rigid particles as toughners. Theoretical analyses developed on encapsulated rigid particle filled composites predicted the effectiveness of a flexible interlayer due to stress relief in the interface region [8, 9]. These works suggest the possibility of toughening, but cannot reflect the real situation in the encapsulated inorganic particle filled polymers. For example, uniaxial tensile stress and linear elasticity conditions assumed in these works are too simplistic. Because of difficulties in the encapsulation of micron-sized particles with rubbery material, not many experiments have been conducted on these types of composites [10–14]. These experiments have their own problems, which will be discussed below. Among them, several studies showed that this core/shell structure does increase the effectiveness of rubber as a toughener [11–13, 15, 16]. However, other studies showed contradictory results, i.e., simple hybrid composites are better for toughening and stiffening than the encapsulated particle filled composites [10, 14, 17]. Furthermore, these previous studies did not focus on the fracture behavior of filled composites and so the underlying mechanism of toughening has never been established. Thus, the effectiveness of this core/shell structure and, particularly, its fracture behavior need to be investigated.

In the current study, the changes in underlying toughening mechanisms due to the existence of rubber interlayers will be examined. This approach is expected to give a common ground for understanding the two previous kinds of studies discussed above. Our work started from the attempted encapsulation of inorganic particles, which was not successful initially. In this step, inorganic particles must be encapsulated with a uniform

* *Present Address*: Department of Chemical Engineering and Materials Science, University of Minnesota, Minneapolis, MN 55455, USA; e-mail: jong@cems.umn.edu.
‡ Author to whom all correspondence should be addressed.

layer of rubber without causing particle agglomeration, and this rubber interlayer must remain stable during subsequent processing. Furthermore, the thickness of the rubber interlayer, which is an important parameter, must be easily controlled.

Approaches such as surface polymerization [18], *in-situ* methods [11, 13, 14, 19–22], and solution/evaporation methods [12, 15] have been attempted, and several modifications of them were tried. The surface polymerization technique involves two steps: immobilization of initiators on the surface of rigid particles and polymerization of rubber from the initiators. This method can yield well-bonded rubber coating on the surface of the glass beads. But in this case, the thickness can be difficult to control.

In the *in-situ* methods, including Hilborn's [11], rubber migrates onto the surface of inorganic particles and forms an interlayer during composite preparation. This technique can improve the uniformity of the rubber interlayer. However, if reactive functional groups, e.g. silane, are used for the rubber migration, it is difficult to preserve the reactive groups until the curing step of the composites [11]. The fraction of reacted groups among the total reactive groups can affect the *in-situ* formation of the rubber interlayer, which depends on thermodynamic and kinetic factors [14]. Because of these two competing factors, this method can give separate rubber phases (rubber particles in matrix) in addition to the rubber interlayer.

The encapsulation method described by Gerard *et al*. [12, 15, 16], a simple solution/evaporation method, usually ends up with severe agglomeration, but this situation is relatively easy to overcome using ball milling and screening techniques. As the rubber interlayer becomes thinner, the aggregates of encapsulated glass beads can be easily broken up. Therefore, in this study, thin rubber-encapsulated inorganic particles are prepared by means of Gerard's method and put into a polymer matrix. The rubbery material for encapsulation is synthesized from carboxyl terminated butadiene acrylonitrile copolymer (CTBN), diglycidyl ether of bisphenol A (DGEBA) epoxide, and isophorone diamine (IPD). The inorganic particles and the polymer matrix are glass beads and epoxy resin, respectively.

Rubber encapsulation has many aspects in common with surface treatment of glass beads. Complete rubber encapsulation will give a totally different interfacial strength between glass beads and matrix. The effect of surface treatment on the fracture toughness of composites is one of the most complicated issues in understanding inorganic particle toughening. Various surface treatments have been developed to improve the interfacial strength between two different phases, especially between inorganic particles and organic matrices. Typical surface treatments used in particulate composites use silane compounds, fatty acids, organotitanates, polymeric compounds, etc. [23, 24]. The actions of these compounds are not simple and more details are available in several references [23, 24].

In most reports on glass bead filled polymers, surface treatments are generally found effective in increasing the interfacial strength between the particles and the matrices, but these surface treatments usually show no significant effect on the fracture toughness of composites [25–28]. Alternatively, surface treatments using releasing agents have also been used to study the effect of weakening the interface between inorganic particles and thermoset matrices on fracture toughness [25, 28]. Interestingly, in most cases, these surface treatments do not significantly affect the fracture toughness of composites [25, 28] either. In some cases, it was found that the fracture toughness actually increases with the decrease of interfacial strength [25, 29]. The results regarding surface treatments are important and intriguing, particularly because the well-accepted toughening mechanism for inorganic particle filled polymers, the crack front bowing mechanism, cannot successfully explain these results [1, 30–36]. The current approach should give new important results on the effect of interfacial strength, which can eventually lead us to understand the major energy absorption mechanisms for inorganic particle filled polymers.

2. Experimental

2.1. Materials

The DGEBA epoxides, DER 332® and DER 661®, are commercial resins produced by the Dow Chemical Co. The CTBN rubber is Hycar 1300 × 13® produced by the BF Goodrich Chemical Co. Two kinds of glass beads are used in this experiment. Both are Speriglass® A-glass beads (sodalime) of Potters Industry Co, but the mean diameter of one (SG) is 3.3 μm and that of the other (LG) is 24.4 μm. Triphenylphosphine, IPD, 4,4′-diaminophenylsulphone (DDS, 98%) and solvents were purchased from the Aldrich Chemical Co, and used without further purification. Glass beads were used after cleaning and drying. Cleaning of glass beads was accomplished by dispersing 290 g of glass beads in 1 L of distilled water under mechanical stirring at room temperature for 6 hours, followed by filtration. This cleaning/filtration process was repeated three times, and glass beads were dried in vacuum at 70 °C for 12 hours. After drying, glass bead aggregates were screened out using a 75 μm sieve (mesh size = 200).

2.2. Preparation of composites

The rubber adduct for the encapsulation of glass beads was prepared in a two-stage process from a CTBN, an epoxide (DER 332®), and IPD following the method of Gerard *et al*. [12, 15], with some modifications. In the first stage, the epoxide was reacted with CTBN at 85 °C for 19 hours (stoichiometric ratio = 0.5) under a nitrogen atmosphere and mechanical stirring, with 0.15 wt% of triphenylphosphine as a catalyst. Chain extension was carried out by adding IPD (stoichiometric ratio = 2) and methylethylketone (MEK/DGEBA = 5 mL/g) at 20 °C. After reacting for a week, the incompletely cured CTBN-DGEBA-IPD (CDI) adduct remains soluble in MEK and could be deposited onto glass beads.

The rubber-encapsulated glass beads were prepared by the solution/evaporation method [12, 15], while changing the feed fraction of the CDI adduct. The glass beads cleaned with distilled water as described before were mixed with the adduct dissolved in MEK

at room temperature for 20 min. Then, MEK was evaporated and the glass beads were dried under vacuum at 120 °C for 12 hours. Under this condition, the secondary amine of IPD can attack the unreacted epoxides in the adduct, resulting in an insoluble network. The rubber-encapsulated glass beads were ball-milled and sieved through 75 μm and 250 μm sieves (mesh size = 200 and 60, respectively) to remove large aggregates. The condition for ball milling was carefully chosen to prevent significant fracturing of glass beads during this pulverizing. In the sieving step, when the only 250 μm sieve was used, the sieved glass beads contained many aggregates. In identifying the glass beads, the letter "w" will be used to indicate a wide size distribution due to the presence of aggregates, e.g. LG(w).

Rubber-encapsulated glass bead filled epoxies were prepared from DER 661®, DDS, and the rubber-encapsulated glass beads. The epoxide resin was first dried under vacuum at 160 °C for 1.5 hours, and mixed with glass beads under the same condition for 1.5 hours. DDS was then mixed with the glass beads/melted epoxide mixture for another 40 min. The degassed mixture was cured in a vertically mounted metal mold in a convection oven at 160 °C for 15 hours and post-cured at 200 °C for 2 hours. During the curing step, glass beads were prevented from settling to the bottom of mold by the relatively high viscosity of epoxide. It was found by thermogravimetric analysis (TGA) that the high viscosity produced no more than 1 vol% void content. The compositions of glass beads filled epoxies are presented in Table I. The epoxy matrix of DER 661®/DDS will be designated as '661'.

2.3. Characterization, fracture toughness assessment and microscopy

Gel permeation chromatography (GPC, Waters 600) was calibrated by using standard polystyrene samples. During the measurements, the flow rate of solvent (tetrahydrofuran) was 1 mm/min. FT-IR data were taken by using Nicolet 5DXB, following standard procedures. For TGA, a TA Instrument SDT 2960 Simultaneous DTA-TGA was used. About 40 mg of sample was heated from 120 °C to 650 °C at 10 °C/min using nitrogen as a balance gas and air as a purge gas.

The mean diameter of glass beads was measured in triplicate by the liquid-phase sedimentation method using a Horiba CAPA-700 particle size distribution analyzer. Glass beads (0.01 wt%) were dispersed in ethylene glycol with hexametaphosphate (0.1 wt%) in ultrasonic bath for 1.5 hours and the mixture was centrifuged by the analyzer. The change in particle concentration on the basis of light transmission was converted into the mean diameter data. The mean diameters of glass beads characterized are given in Table II.

The designation of glass beads, which can be found in Table II, indicates the size of glass beads and the feed fraction of CDI adduct in the solution/evaporation encapsulation step. The number in front of the hyphen is the feed fraction (wt%) of CDI adduct, so the thickness of CDI adduct layer in composites increases with this number. As for the designations of all encapsulated SG and LG systems, r-SG and r-LG will be used respectively, where 'r' indicates rubber encapsulation.

For fracture toughness assessment, single-edge-notched (SEN) type specimens were fractured in three-point bend (3PB) geometry (span, $S = 50.8$ mm) using a screw-driven Instron machine (Instron 4502). The crosshead speed of 3PB test was 2.54 mm/min. SEN type specimens (thickness (B) = 6.35 mm and width (W) = 12.7 mm) were prepared, and a sharp notch was introduced by tapping a hammer on a razor blade inserted into the specimen. Before a razor blade was inserted into a specimen, the blade was cooled in liquid nitrogen until boiling around it stopped. The sharp notch introduced in this manner was always longer than the insertion length of razor blade. For each composition, twelve to eighteen specimens were prepared and tested. Critical stress intensity factor (K_{IC}) and critical strain energy release rates (G_{IC}) were calculated using these relationships:

$$K_{IC} = Y\frac{3PS\sqrt{a}}{2BW^2} \quad (1)$$

$$Y = 1.93 - 3.07\left(\frac{a}{W}\right) + 14.53\left(\frac{a}{W}\right)^2 - 25.11\left(\frac{a}{W}\right)^3 + 25.80\left(\frac{a}{W}\right)^4$$

$$G_{IC} = \frac{K_{IC}^2}{E} \quad (2)$$

where Y is a shape factor, P is the load at failure, and a is the crack length. Although Equation 2 gives G_{IC}

TABLE I Formulations of various toughened epoxies

Component	Composition (phr)[1]
DER 661®	100
DDS	12.2
Glass Beads[2]	0, 4.8, 12.3, 26, 58.5

[1]phr = Parts per hundred of epoxide by weight.
[2]Weight of only glass beads except CDI adduct layers.

TABLE II Mean diameter of various kinds of glass beads used in this experiment obtained by using a particle size analyser

Glass Beads	SG	0.5-SG	1.5-SG	3.0-SG	4.5-SG	6.0-SG
Mean Diameter (μm)	3.3	6.6	9.6	17.6	17.0	21.6
Glass Beads	LG	0.5-LG	1.5-LG	3.0-LG	—	—
Mean Diameter (μm)	24.4	29.6	25.5	39.0	—	—
Glass Beads	—	0.5-LG (w)	1.5-LG (w)	3.0-LG (w)	4.5-LG (w)	—
Mean Diameter (μm)	—	34.4	37.9	49.4	91.6	—

values in the plane stress condition, the use of this equation does not change our conclusions on the effect of rubber interlayer, as will be explained later. After the fracture toughness test, the fracture surface of specimens was examined using a scanning electron microscope, Hitachi S-800, at an accelerating voltage of 5 or 3 kV. For this microscopy study, the fracture surface was coated with a thin layer of gold-palladium.

For understanding the fracture process of glass bead filled epoxies, sub-critically loaded cracks were prepared by using the double-edge-notched four-point bend (DEN-4PB) technique [37]. Then, thin-sections containing the cracks were taken and examined using an optical microscope (OM), Nikon Microphot II. The DEN-4PB technique is well described elsewhere [37]. This technique enables the preparation of sub-critically loaded cracks by fracturing specimens having two almost identical cracks on the same edge in the four-point bend geometry. The two cracks cannot be completely identical, and so one of them will break while the other experienced sub-critical (just before failure) loading. Thin-sections of about 40 μm thickness were taken from the mid-planes of the specimens using the petrographic thin-sectioning technique [38–40]. Rough to fine silicon carbide (SiC) grinding discs (grit size 80, 250, 400, 600, 1000) and alumina suspensions (5, 1, 0.3, 0.05 μm) were used for polishing. At least two sections were prepared for a composition of epoxy resin. The surface artifacts [40] generated from the polishing was identified using a reflected light OM before the investigation on sub-critically loaded cracks. Sub-surface damages in SEN-3PB specimens were also examined by using the same thin-sectioning technique.

Uniaxial tensile specimens (gauge section $= 15 \times 5 \times 7$ mm) whose surface was polished using SiC grinding discs (grit size 600), were also tested. The average modulus value of an epoxy resin was obtained from the test results of more than five specimens. The same screw-driven Instron machine was used at a crosshead speed of 2.54 mm/min.

3. Results and discussion

3.1. Encapsulation of glass beads with CDI adduct

The first step for encapsulation is the synthesis of CDI adduct. Gerard's method [12, 15] is modified by the addition of MEK at the second step. A small amount of MEK (MEK/DGEBA = 5 mL/g) is used at the second step, because the viscosity of the DGEBA-CTBN adduct is too high to be homogeneously mixed with IPD in the second step. Since the addition of MEK may retard the reaction between IPD and DGEBA-CTBN adduct, the final CDI adduct was used after reacting for a week.

Fig. 1 shows the results of GPC and FT-IR which were used to characterize the incompletely cured CDI adduct as in ref 12. In Fig. 1A, size exclusion chromatography (SEC) trace shows a single but broad peak. This result proves that the adduct is not monodisperse, but does not contain a significant amount of

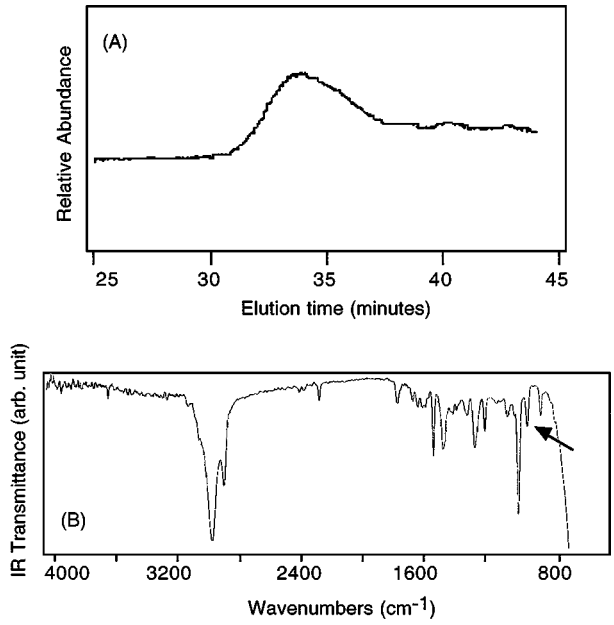

Figure 1 Analysis on CDI adduct before complete cross-linking: (A) SEC traces (Mn = 7500, Mw = 14500, polydispersity = 1.94); (B) FT-IR (note the peak at 910 cm^{-1} that indicates the existence of oxirane).

unreacted monomers. Although most monomers are thought to be consumed, the existence of unreacted epoxide rings (oxirane) can be found around 910 cm^{-1} in the FT-IR spectrum shown in Fig. 1B. From these two characterizations, it is confirmed that the incompletely cured adduct which has unreacted epoxide functional groups, is successfully prepared. The unreacted epoxide groups in the adduct are supposed to enhance the interfacial strength between the adduct layer and epoxy matrix in composites through mainly the chemical reactions between them and the amines of curing agents [12, 15]. Besides GPC and FT-IR, FT-NMR was used as well to characterize the CDI adduct. Although the FT-NMR spectrum of the CDI adduct was found to be complicated, the peak of unreacted epoxide rings was found around 3.8 ppm to indicate the presence of oxirane.

After the incompletely cured CDI adduct was prepared, it was used to encapsulate glass beads using the solution/evaporation method [12, 15, 16]. After this encapsulation step, the incompletely cured CDI layers were completely cured at 120 °C. The glass transition temperature (T_g) of completely cured CDI adduct measured using DSC (differential scanning calorimetry) was −24 °C and its density was 1.01 g/cm^3. On the other hand, T_g of the CTBN liquid rubber used in the preparation of CDI adduct was −36 °C and its density was 0.96 g/cm^3 [41]. It is obvious and, in fact, expected that there would be an increase in T_g and density due to the cross-linking reaction.

The existence of CDI adduct layers is confirmed by using TGA (Fig. 2) and SEM (Fig. 3). Fig. 2 shows that the weight fraction of rubber layers measured by TGA follows the increase of their feed fraction. This simple relationship can be expected, because the solution/evaporation method is simple. The t/r (thickness of rubber layer/mean radius of glass beads) data in Fig. 2 are calculated from the weight fraction of CDI adduct

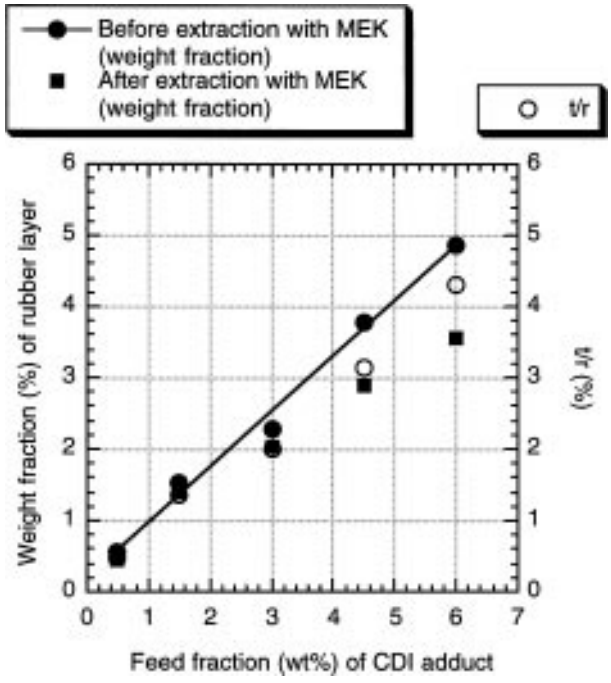

Figure 2 Weight fraction of the rubber layer on glass beads versus the feed fraction of CDI adduct. The ratio, t/r, is thickness of rubber layer/mean radius of glass beads.

and the densities of glass beads and completely cured CDI adduct.

Before the final curing step of the CDI layer, the CDI adduct was soluble in MEK, but after curing, it became almost insoluble. Results showing this solubility change can be found in Fig. 2 (also Fig. 3D). After the extraction of cured CDI layers with MEK, the weight fraction of rubber layers decreased only a little. This experiment on solubility confirmed the existence of a stable CDI layer for the preparation of composites. For the extraction, encapsulated glass beads were first dispersed in MEK under mechanical mixing for 30 min and then MEK was filtered out. During this extraction, a significant amount of CDI adduct fragments which can be produced by mainly ball-milling can be filtered out, if their size is smaller than the filter pores. Accordingly, the decrease in the weight fraction of rubber layer due to the extraction increases significantly, as the feed fraction increases (Fig. 2).

The other method to confirm the existence of rubber layers is by the use of SEM. All three micrographs of glass bead (SG) surfaces in Fig. 3 except the micrograph (A) directly show the existence of rubber layers. Although the layers are not of uniform thickness and many aggregates obviously exist, the rubber layers found in (B), (C) and (D) are fairly well spread out over the surface of glass beads. In fact, there is continuity in and among the rubber layers: A coating on a glass bead is found to be smoothly connected with the coating on the next glass bead. Consequently, the encapsulation of glass beads appears to have been successfully performed. Furthermore, in Fig. 3A, the CDI adduct appears to be spread out over the surface of glass beads forming a very thin and rather uniform layer, which is not easily discerned. TGA analysis proved the existence of the layers in 0.5-SG of Fig. 3A. Since the encapsulation will change the surface chemical composition of glass beads, X-ray photoelectron spectroscopy (XPS) was also used to confirm the encapsulation. Its result showed that the concentration of carbon species was higher on the surface of encapsulated glass beads than that of uncoated glass beads. However, because of the carbonaceous overlayer on the uncoated glass bead surface [42], a quantitative comparison is not possible.

As seen in Fig. 3, more aggregation results from the encapsulation as the feed fraction of CDI adduct increases. As a simple way to characterize the degree of aggregation, the size distribution measurement by the liquid-phase sedimentation method was performed in triplicate. The size distribution curves obtained from this method show the equivalent diameter of aggregates, because it assumes perfectly spherical shape of particles. The mean diameters are given in Table II. As a rule, the mean diameter increases with increasing feed fraction of CDI adduct. The increase appears to be more systematic and noticeable in small glass bead (r-SG) systems than in large glass bead (r-LG) systems (see also Fig. 3).

3.2. Mechanical properties of composites

The K_{IC} data of rubber-encapsulated glass bead filled epoxies are shown in Fig. 4. First of all, there is no significant increase or decrease of K_{IC} compared to the error ranges regardless of t/r values. (The error range is the standard deviation of experimental data.) There is only a slight increase or decrease of K_{IC}. Therefore, thickness of the rubber interlayer (t) does not appear to have any significant influence on K_{IC}. Furthermore, the comparison between the fracture toughness data of r-LG and r-LG(w) systems in Fig. 4 proves that the degree of aggregation does not have any significant influence on K_{IC} either.

The effect of rubber encapsulation on K_{IC} with changing glass bead content is presented in Fig. 5. While K_{IC} distinctly increases with the increase in glass bead content, there is no effect on K_{IC} from the rubber encapsulation and the degree of aggregation. This result agrees well with the results of Fig. 4. G_{IC} data in Fig. 6 support this result as well. Although, with increasing t/r, G_{IC} slightly increases in r-SG/661 systems and slightly decreases in r-LG/661 and r-LG(w)/661 systems, these changes are not large enough to show a significant effect of rubber encapsulation and aggregation. In fact, the G_{IC} data in Fig. 6 convey the same information as that in Fig. 4. This is because the modulus of these composites does not change significantly within the ranges of thickness of rubber interlayer and the degree of aggregation (Fig. 7).

These results are surprising, because several groups [10–16] report an increase in the fracture toughness of encapsulated-particle filled composites due to the existence of rubber interlayers, while others [11–13] show a decrease [10, 14, 17]. Unfortunately, in these reports, no information on the degree of aggregation was given, and the matrices and the rubbery materials are different from those used here. Therefore, it is difficult to directly compare our data with those of others. It can

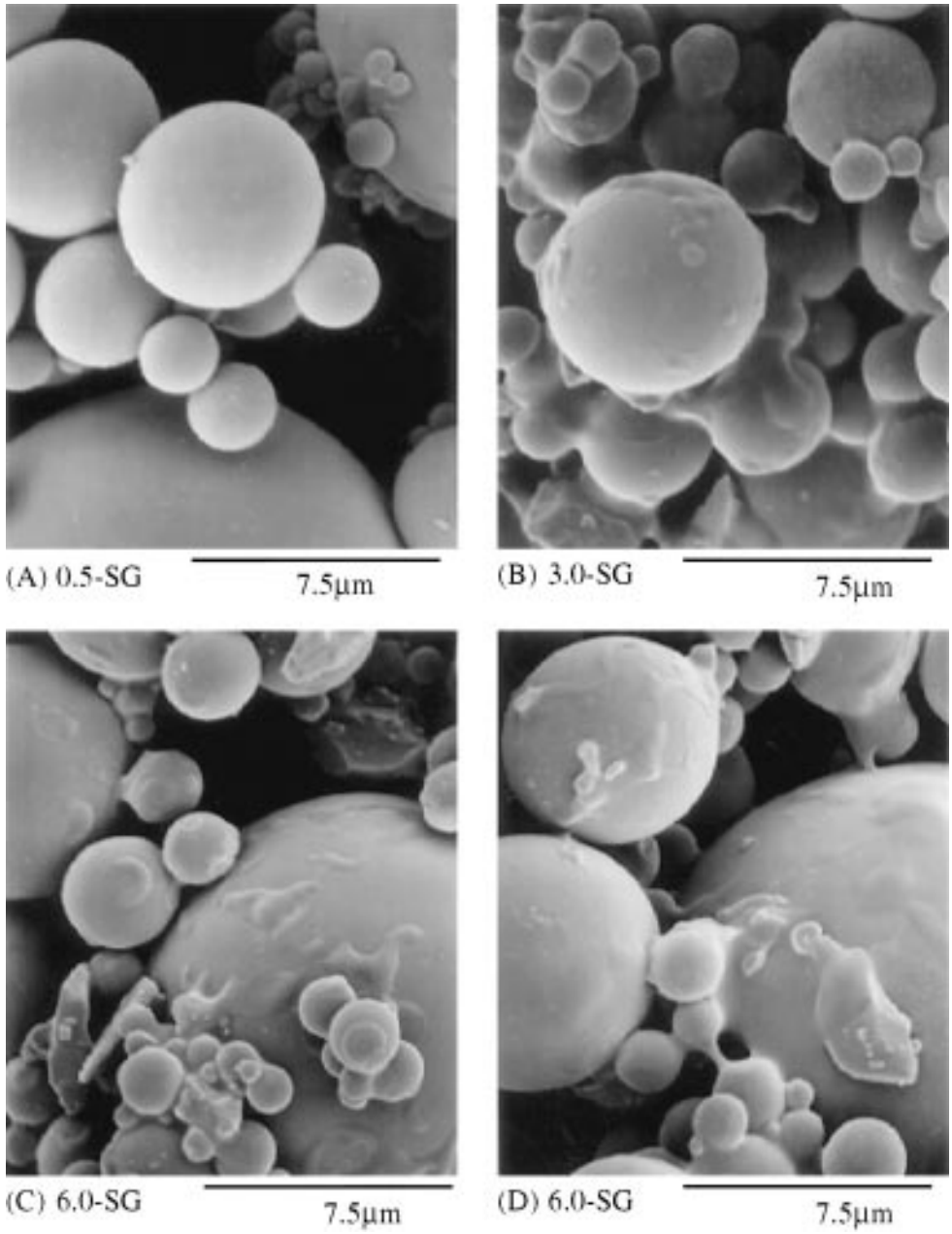

Figure 3 SEM micrographs of the glass beads (SG) that are encapsulated with changing the feed fraction of CDI adduct: (A) = 0.5 wt%; (B) = 3.0 wt%, (C) = 6.0 wt% before the extraction with MEK; (D) = 6.0 wt% after the extraction with MEK.

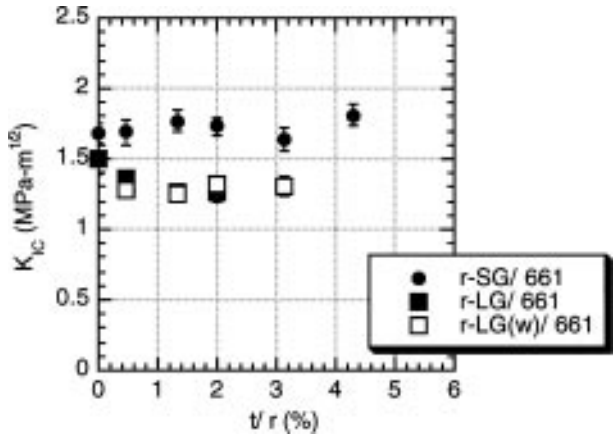

Figure 4 Effect of the thickness of a rubber interlayer on the critical stress intensity factor for epoxies filled with rubber-encapsulated glass beads: $t/r(\%)$ = thickness of rubber interlayer/mean radius of glass beads. (content of glass beads = 58.5 phr in r-SG/661, and 26 phr in r-LG/661 and r-LG(w)/661.)

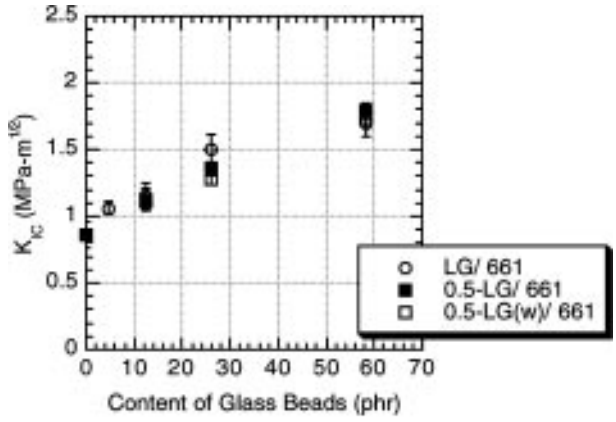

Figure 5 Critical stress intensity factor of rubber-encapsulated glass bead filled epoxies versus glass beads content.

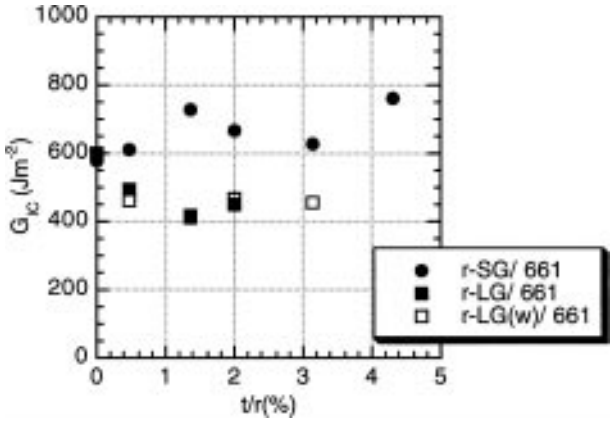

Figure 6 Effect of the thickness of a rubber interlayer on the critical strain energy release rate of epoxies filled with rubber-encapsulated glass beads: t/r(%) = thickness of rubber interlayer/mean radius of glass beads. (Content of glass beads = 58.5 phr in r-SG/661, and 26 phr in r-LG/661 and r-LG(w)/661.)

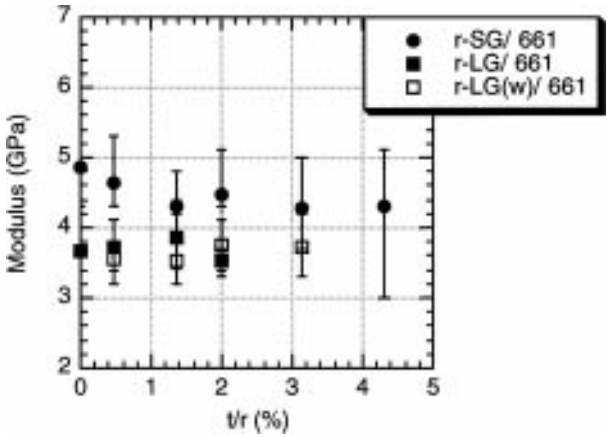

Figure 7 Effect of the thickness of a rubber interlayer on the tensile modulus of epoxies filled with rubber-encapsulated glass beads: t/r(%) = thickness of rubber interlayer/mean radius of glass beads. (Content of glass beads = 58.5 phr in r-SG/661, and 26 phr in r-LG/661 and r-LG(w)/661.)

be stated only for the epoxies prepared here that neither the rubber encapsulation nor the aggregation of glass beads significantly affect the fracture toughness of the composites.

The tensile modulus data of encapsulated glass bead filled composites versus t/r are presented in Fig. 7. As already mentioned above, there is no significant change of modulus due to the rubber encapsulation and the degree of aggregation. The moduli of all r-SG and r-LG systems lie well between the upper and lower bounds calculated by the equations proposed by Ishai and Cohen [43] (5.8–4.1 GPa for r-SG systems and 4.6–3.3 GPa for r-LG). Since modulus is a material property measured at very small strains, it seems possible that neither the thin rubber layer around glass beads nor the aggregates of encapsulated glass beads can significantly decrease the modulus of composites. In Fig. 7, the very small decrease of modulus with increase of t/r and the relatively large error range of the modulus of r-SG/661 systems might lead us to suspect the influence of aggregates (inhomogeneous dispersion). Since r-SG has a higher degree of aggregation than in r-LG, the large error range seems to be more noticeable in the r-SG systems than the r-LG systems.

3.3. Microscopy Study I - SEM micrographs

Up to now, no noticeable effect of rubber encapsulation and aggregation has been found. However, SEM microscopy study on fracture surface reveals significant changes in micro-mechanical deformations, particularly debonding of glass beads, due to the rubber encapsulation.

For easy comparison with non-encapsulated systems, interfacial strength and debonding in encapsulated systems will be defined as follows. The interfacial strength in encapsulated systems is the critical stress or strain to cause one of two interfaces in encapsulated systems to fail, one between glass beads and rubber interlayers, and the other between rubber interlayers and matrix. Therefore, debonding or interfacial failure in encapsulated systems means the failure of stress transfer between glass beads and matrix.

Micrographs of the fracture surface of LG/661 and 0.5-LG/661 are in Fig. 8. Step structures in the encapsulated system ((B) and (D)) are as noticeable as in the non-encapsulated system ((A) and (C)). Debonding zone size is wider in the encapsulated system than in the non-encapsulated system. Average debonding zone sizes measured using more than 15 OM and SEM micrographs are 54 ($\pm$13) and 125 ($\pm$53) μm for LG/661 and 0.5-LG/661, respectively. The decrease of interfacial strength due to the rubber encapsulation is evident in the SEM micrographs from the fast-fracture regions; Fig. 8D and F show more adhesive failure than Fig. 8C and E.

Aggregation becomes more prevalent in thicker rubber interlayer systems. While the fracture surface of 3.0-LG/661 in Fig. 9A shows a small aggregate, thicker interlayer systems are found to have much larger aggregates as the fracture surface of 0.5-LG(w)/661 shows in Fig. 9B. Investigation of the inside of aggregates at higher magnification, Fig. 9C and D, shows that the interstitial sites between glass beads are well filled with epoxy resin. As can be seen in non-encapsulated systems, plastic dilatation of the matrix around debonded glass beads can also be found in these micrographs. In addition to this matrix dilatation, the drawing of a rubber layer between glass beads is evident in Fig. 9D. The residual strain in this layer seems to be larger than that in the dilated matrix.

An interesting feature seen in Fig. 9D is that the debonding of glass beads from the matrix occurs at the interface between rubber and epoxy, not at the interface between rubber and glass. Since epoxide functional groups can exist in rubber layers, the interface between the layers and matrix can be strengthened by chemical reactions between these groups and amine functional groups in the matrix [12, 15]. On the other hand, the interface between glass and rubber might not have as strong chemical linkages as the other interface. Contrary to this reasoning, debonding mostly occurs at the interface between rubber and matrix. It is possible that the shrinkage of CDI adduct during encapsulation and curing processes is a reason for the unexpectedly strong interface between glass and rubber. Functional groups on the glass surface, such as hydroxyls, might also strengthen the interface by

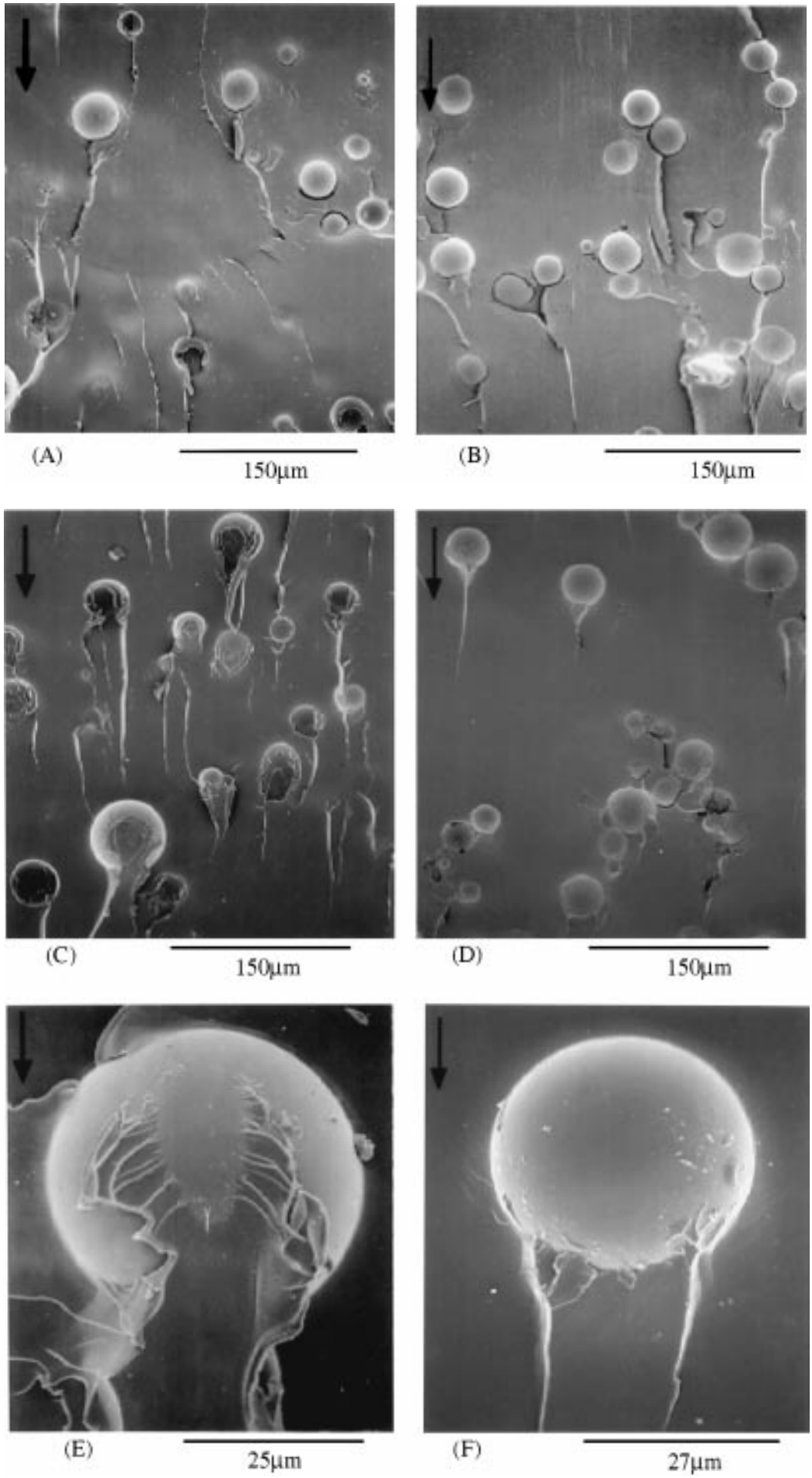

Figure 8 SEM micrographs of the fracture surface of SEN-3PB specimens of (A), (C) and (E) 26 phr LG/661 and (B), (D) and (F) 26 phr 0.5-LG/661: (A) and (B) process zone; (C), (D), (E) and (F) fast fracture region. The arrows indicate the direction of crack propagation.

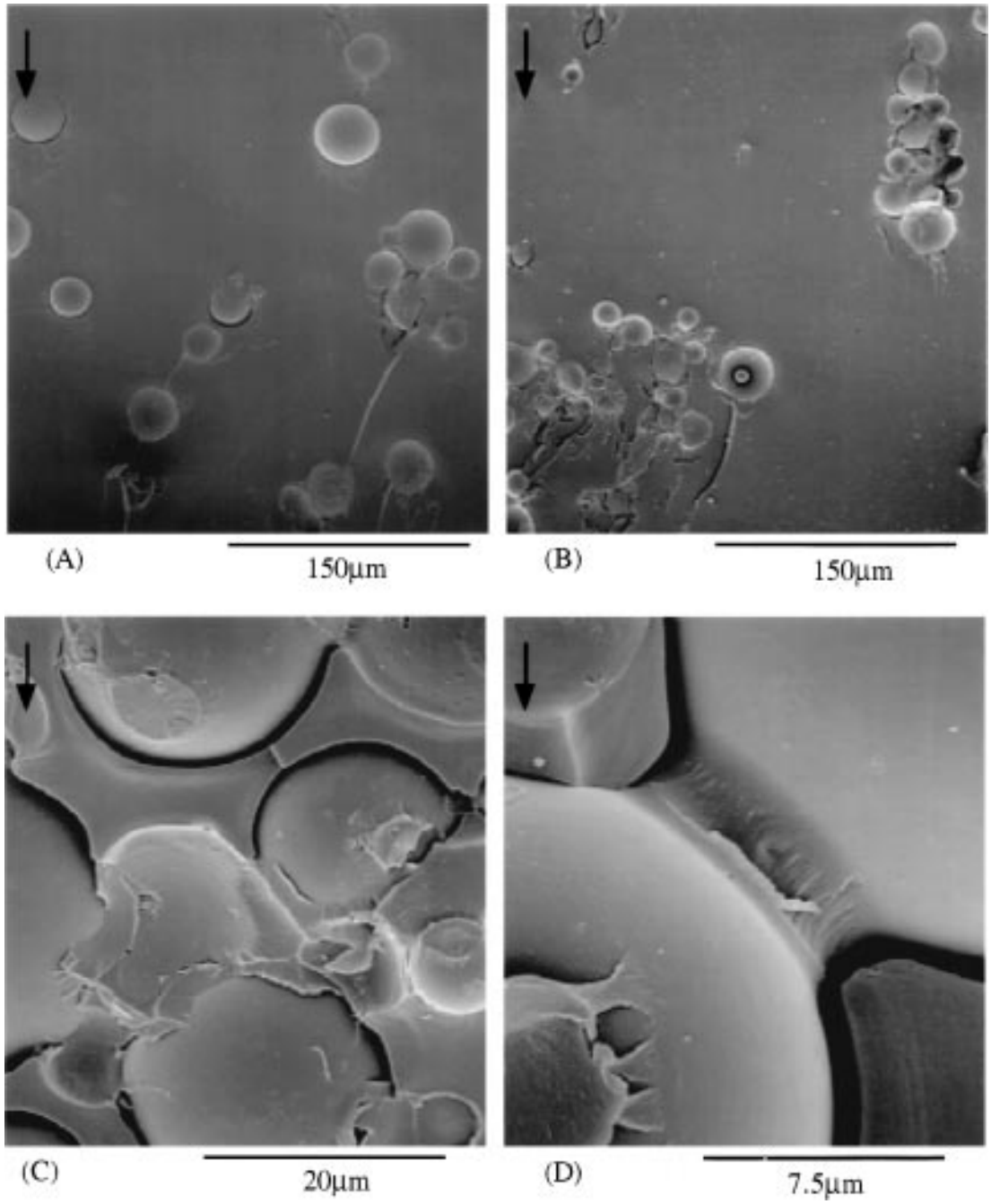

Figure 9 SEM micrographs of the fracture surface of SEN-3PB specimens (process zone): (A) 26 phr 3.0-LG/661; (B), (C) and (D) 26 phr 0.5-LG(w)/661. The arrows indicate the direction of crack propagation.

interacting with functional groups in rubber, such as amines.

The results of SEM micrographs show that encapsulated glass beads can more easily debond from the matrix than non-encapsulated glass beads. Yet, the fracture toughness of composites does not reflect this decrease in the interfacial strength. The same conclusion has been obtained from the previous researches [25–28] on the effect of silation, which is that the surface treatments of glass beads can affect micro-deformations occurring during fracture but not the fracture toughness of composites.

It is also worth mentioning that the areal density of characteristic tails (the major type of step structure in our systems) behind glass beads decreases as aggregation becomes more severe (Fig. 8A and Fig. 9A and B). This is because an aggregate cannot play a role of more than a split point, i.e. a point that divides the primary crack front into two secondary crack fronts. Consequently, the areal density of split points available will decrease as more aggregation results from the encapsulation of glass beads. In the crack front bowing mechanism, the split point in here is the pinning point [4, 31–36]. When two secondary cracks generated by a pinning point meet with each other, the characteristic tail structure is formed.

3.4. Microscopy Study II - OM micrographs

Interestingly, our OM study on sub-surface micromechanical deformations provides the salient features of fracture. Because of the macroscopically brittle fracture behavior of glass bead filled epoxies, fractographic investigation on fracture surface have been more performed than sub-surface investigation.

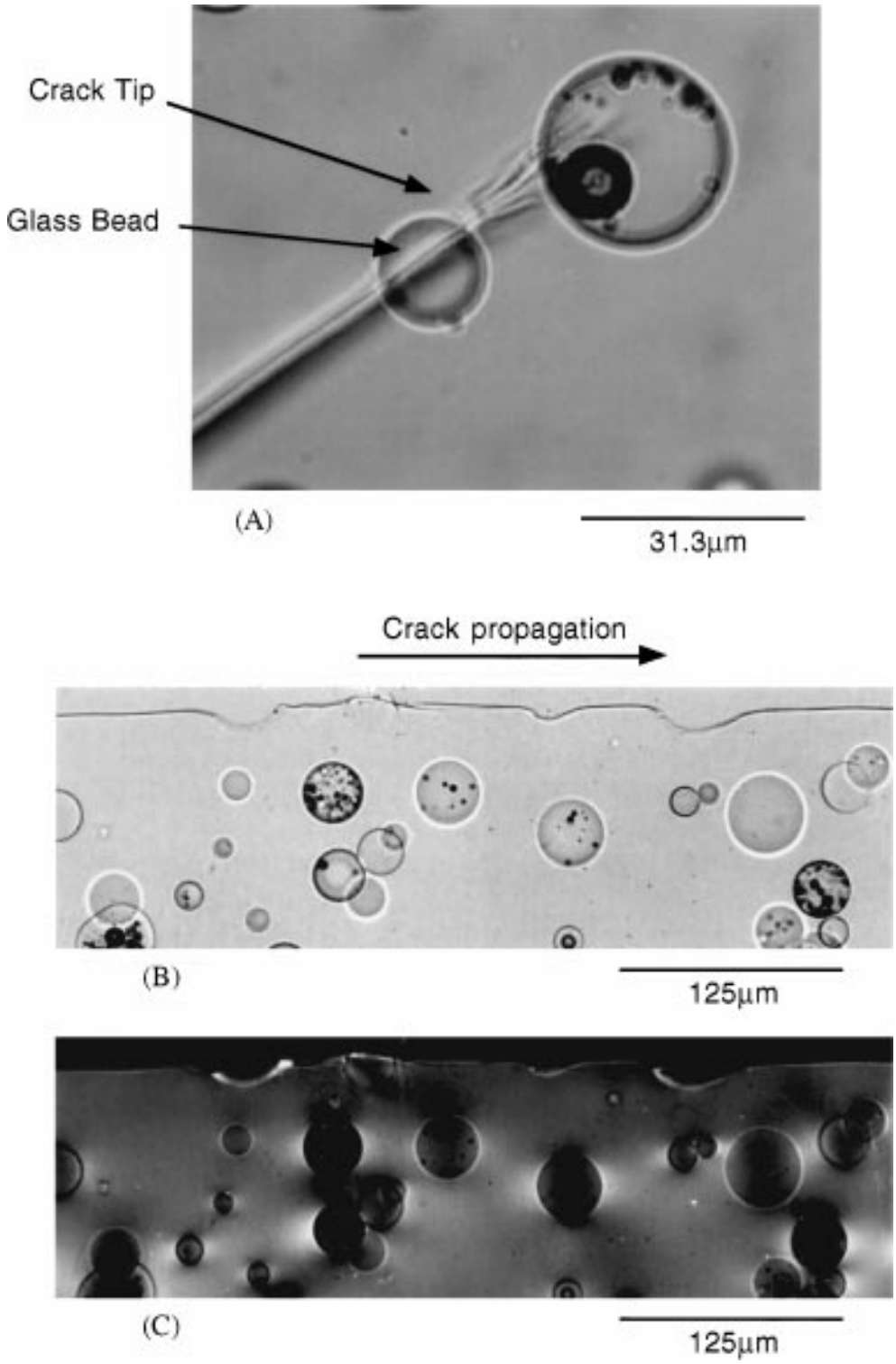

Figure 10 Transmitted light optical micrographs of thin sections of 26 phr LG/661: (A) tip of a sub-critically loaded crack in a DEN-4PB specimen; (B) process zone in a SEN-3PB specimen (without polarizers); (C) the same region as that in (B), but between crossed polarizers.

Figs 10–12 show optical micrographs of the sub-surface damages in composites containing relatively little aggregation, and Fig. 13 shows the sub-surface damages around large aggregates. In Figs 10 and 11, micro-shear bands [44–46] (fine dark lines) developed in a sub-critically loaded crack tip region can be found. These micro-shear bands were clearly identified using several experiments [47, 48]. They were found to be removable by heating up to about 10 °C below the T_g of the matrix. Furthermore, SEM and OM micrographs show neither cracks [49] nor crazes in the location of the dark lines (micro-shear bands). In addition to micro-shear bands, debonding of glass beads can also be found in Figs 10 and 12 as indicated by the crater structures. The glass bead at the bottom right corner of Fig. 11A is surrounded by concentric semicircles, which can also indicate that debonding had occurred.

In Figs 10–12, there are birefringent regions around craters indicating diffuse matrix shear yielding. This birefringence is more intense around the equatorial region of 'craters'. (The equatorial region refers to the interfacial region between glass beads and the matrix parallel to the direction of the far-field stress.) This is because stress is inevitably amplified at these

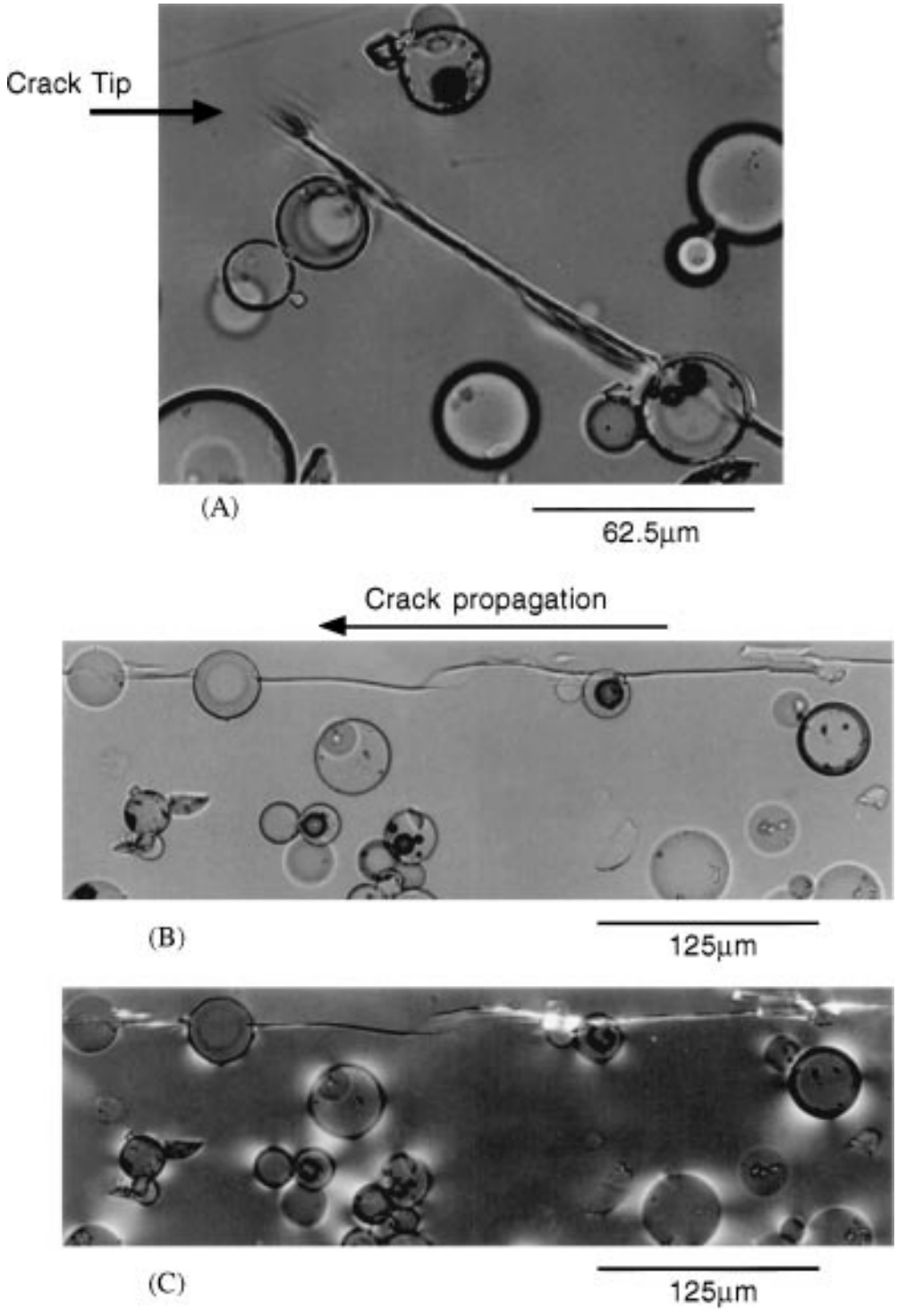

Figure 11 Transmitted light optical micrographs of thin sections of 26 phr 0.5-LG/661: (A) tip of a sub-critically loaded crack in a DEN-4PB specimen; (B) process zone in a SEN-3PB specimen (without polarizers); (C) the same region as that in (B), but between crossed polarizers.

regions after debonding of glass beads [50]. This explanation is based on the assumption that shear yielding is initiated by debonding of glass beads. In addition to debonding, mixed mode stress conditions during crack propagation around glass beads can initiate matrix shear yielding as well [51, 52]. Since mixed mode character will be a maximum around the equatorial region, the intense birefringence can be expected. Nonetheless, Figs 11 and 12 supports the first explanation that the diffuse shear yielding of the matrix is initiated by the debonding of glass beads. This is because the mode II or III stress components of the fracture around the shear yielded regions in these micrographs appear to be too small to be able to cause the matrix to yield.

Since the two mechanisms, debonding of glass beads and diffuse matrix shear yielding, can be related with each other as described above, they can be treated as a combined mechanism. It was found in the previous section on SEM micrographs that the size of debonding zone increased as the thickness of rubber interlayers increased. Thus, debonding/diffuse matrix shear yielding will also increase, and more fracture energy will be dissipated through this mechanism.

Similar to non-encapsulated systems, encapsulated systems exhibit the birefringent features generated by

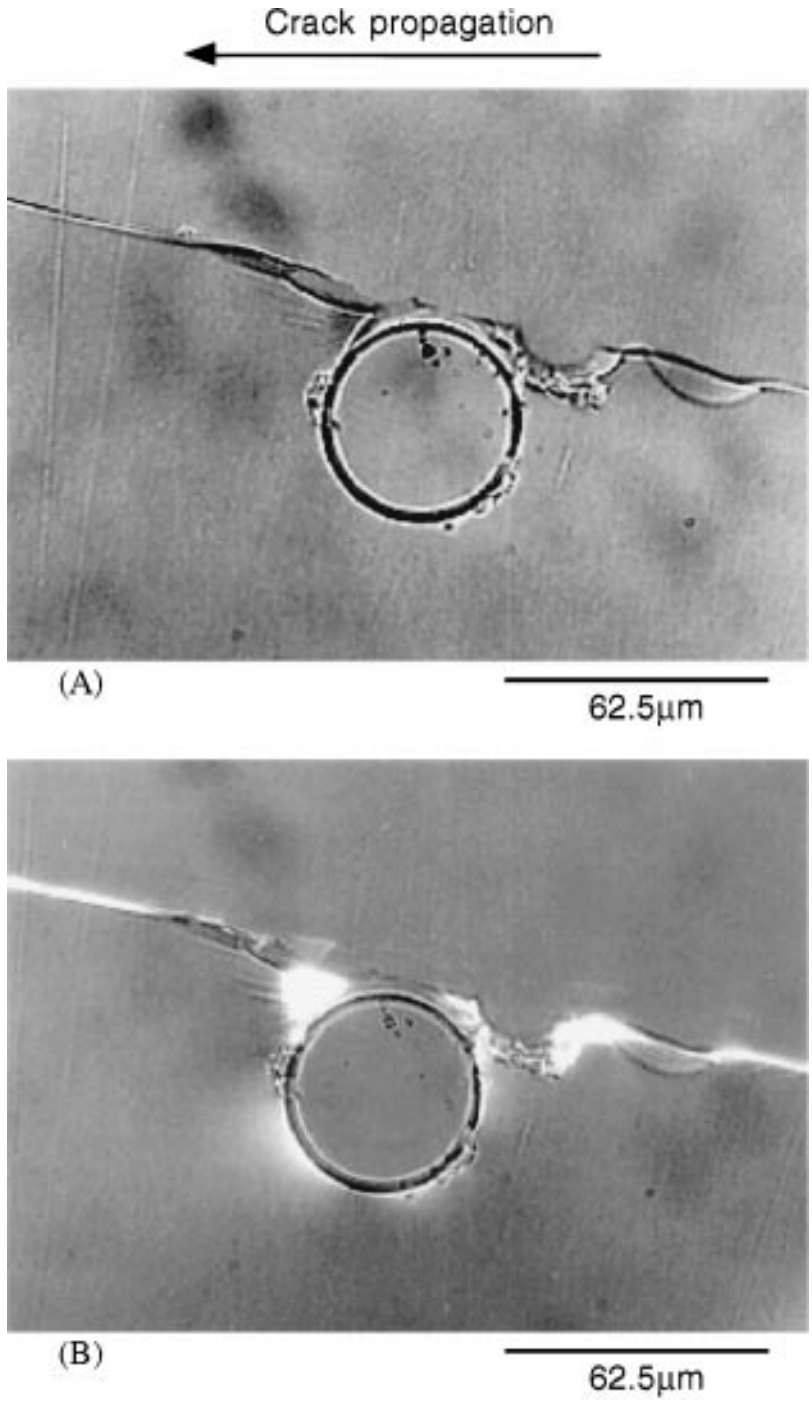

Figure 12 Transmitted light optical micrographs of a thin section taken in process zone of a SEN-3PB specimen of 26 phr 3.0-LG/661: (A) without polarizers; (B) the same region as that in (A), but between crossed polarizers.

thermal residual misfit [53–55] (Figs 10–12). However, it is not clear in here whether the thin rubber layers between glass beads and matrix can significantly relieve thermal residual misfit in the matrix or not.

Fig. 13 shows the sub-surface damage in composites containing a significant number of aggregates. Micro-shear bands are still observable around aggregates at the crack tip region (Fig. 13B). However, the size of the micro-shear band zone is not proportional to the number of glass beads inside the aggregate. In non-encapsulated systems, each glass bead at the crack tip region has micro-shear bands developed around it. Thus, the energy absorption via micro-shear banding will be smaller as the degree of aggregation increases. Micrograph (A) might bring us the conjecture that crack bridging by aggregates might be possible.

The contribution of debonding/diffuse matrix shear yielding seems able to answer the question why the fracture toughness of composites remains constant while the thickness of rubber interlayer (or degree of aggregation) increases. (Unfortunately, the two variables, thickness of rubber interlayer and the degree of aggregation, were not clearly separated in this experiment (Table II). Although 0.5-LG does not contain a significant amount of aggregation, the comparison between LG/661 and 0.5-LG/661 is not enough to understand the effect of thickness change separately from the effect of aggregation.) The energy absorption due to debonding/diffuse

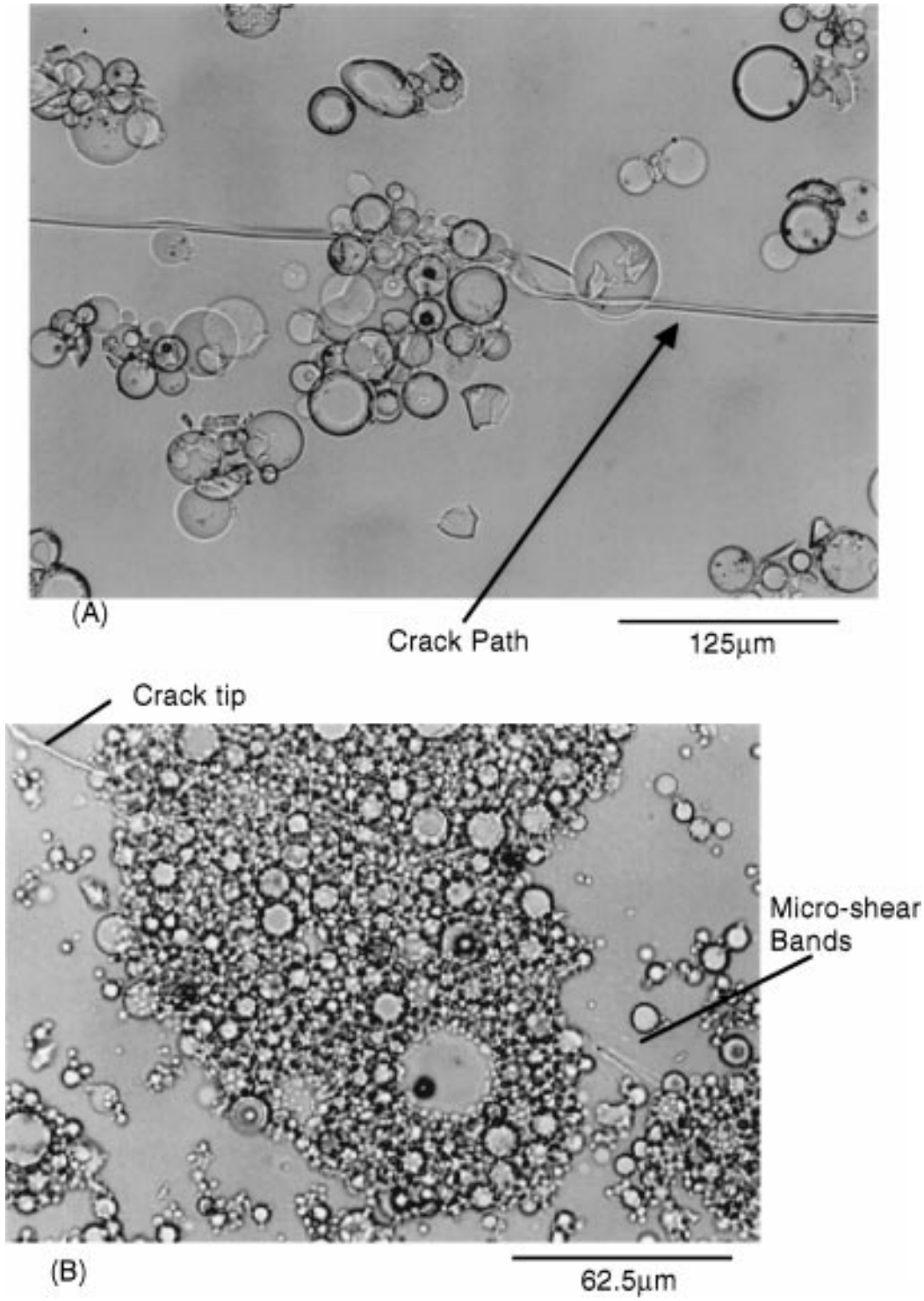

Figure 13 Optical micrographs of thin sections taken near the tip of sub-critically loaded cracks in DEN-4PB specimens: (A) 26 phr 0.5-LG(w)/661; (B) 58.5 phr 3.0-SG/661.

matrix shear yielding are found to increase as the thickness of rubber interlayers (or degree of aggregation) increases. On the other hand, the energy dissipation due to the other mechanisms, step formation and micro-shear banding, are found to decrease as the thickness increases. Consequently, no significant decrease or increase of toughness can occur (Figs 4–6). The previous controversial results on the effect of rubber interlayers on toughening might be caused by different offsetting between the two mechanisms, i.e. one favorable and the other adverse.

It seems to be the case that future research must focus on how to enhance the favorable effect. For example, more ductile epoxy matrix can be expected to enhance diffuse matrix shear yielding and micro-shear banding, resulting in more effective toughening. This surmise was found to be true in our experiments, which will be reported in future.

4. Conclusions

Rubber-encapsulated glass bead filled epoxies were prepared and their fracture behavior was investigated in detail to understand the effect of rubber encapsulation. Glass beads were encapsulated with a synthesized rubber by using the solution/evaporation method and subsequent curing [12]. As the thickness of the

rubber layer increased, the degree of aggregation increased, though controlled by milling and sieving. The fracture toughness, K_{IC} and G_{IC}, and modulus of composites were found to be marginally affected by rubber encapsulation and aggregation. Rubber encapsulation was observed to decrease the interfacial strength between glass and matrix. Between the two interfaces in rubber-encapsulated glass bead filled epoxies, that between rubber and matrix was found to fail first upon crack propagation.

Several possible energy dissipating mechanisms were identified: step formation, debonding of glass beads, diffuse matrix shear yielding, and micro-shear banding. The diffuse matrix shear yielding was initiated by the debonding of glass beads. Among the energy absorbing deformations, the step formation and the micro-shear banding were found to decrease as the thickness of rubber layer increased. On the other hand, the debonding/diffuse shear yielding was found to increase with the increase in layer thickness. The lack of influence of rubber encapsulation on the fracture toughness of composites could be understood by the offsetting effects of several mechanisms.

Acknowledgements

This work was supported by the Specialized Materials Science Research Center of National Institute of Health (NIH), under a contract No. DEO 9296-09. Authors would like to thanks Dr. Jimmy Kishi, Dr. Jack Huang, and Jacqueline M. Denoyer for their help.

References

1. A. J. KINLOCH and R. J. YOUNG, "Fracture Behavior of Polymers" (Elsevier Applied Science, 1985).
2. C. VIPULANANDAN and S. MEBARKIA, *J. Appl. Polym. Sci.* **50** (1993) 1159.
3. L. NICOLAIS, E. DRIOLI and R. F. LANDEL, *Polymer* **14** (1973) 21.
4. A. J. KINLOCH, D. L. MAXWELL and R. J. YOUNG, *J. Mater. Sci.* **20** (1985) 4169.
5. A. C. MOLONEY, H. H. KAUSCH, T. KAISER and H. R. BEER, *ibid.* **22** (1987) 381.
6. R. J. YOUNG, D. L. MAXWELL and A. J. KINLOCH, *ibid.* **21** (1986) 380.
7. H. ZHANG and L. A. BERGLUND, *Polym. Eng. Sci.* **33** (1993) 100.
8. V. A. MATONIS and N. C. SMALL, *ibid.* **9** (1969) 90.
9. L. J. BROUTMAN and B. D. AGARWAL, *ibid.* **14** (1974) 581.
10. G. F. ABATE and D. HEIKENS, *Polym. Comm.* **24** (1983) 137.
11. J. HILBORN, J. BIDAUX and J. E. MANSON, *Polymer Preprint* **34** (1993) 639.
12. Y. G. LIN, J. F. GERARD, J. Y. CAVAILLE, H. SAUTEREAU and J. P. PASCAULT, *Polym. Bull.* **17** (1987) 97.
13. C. SCOTT, H. ISHIDA and F. H. J. MAURER, *J. Mater. Sci.* **22** (1987) 3963.
14. J. KOLARIK and J. JANCAR, *Polymer* **33** (1992) 4961.
15. N. AMDOUNI, H. SAUTEREAU and J. F. GERARD, *J. Appl. Polym. Sci.* **45** (1992) 1799; *ibid.* **46** (1992) 1723.
16. N. AMDOUNI, H. SAUTEREAU, J. F. GERARD, F. FERNAGUT, G. COULON and J. M. LEFEBVRE, *J. Mater. Sci.* **25** (1990) 1435.
17. M. E. J. DEKKERS, J. P. M. DORMANS and D. HEIKENS, *Polym. Comm.* **26** (1985) 145.
18. T. SUGAWARA and T. MATSUDA, *Macromolecules* **27** (1994) 7809.
19. B. PUKANSZKY, F. TUDOS, J. KOLARIK and F. LEDNICKY, *Polym. Compos.* **11** (1990) 98.
20. J. KOLARIK, F. LEDNICKY, J. JANCAR and B. PUKANSZKY, *ibid.* **31** (1990) 201.
21. J. JANCAR and A. T. DIBENEDETTO, *J. Mater. Sci.* **29** (1994) 4651.
22. D. BENDERLY, A. SIEGMANN and M. NARKIS, *Polymer Composites* **17** (1996) 86.
23. R. ROTHON, "Particulate-filled Polymer Composites" (Longman Scientific & Technical, 1995).
24. E. P. PLUEDDEMANN, "Silane Coupling Agent" (Plenum, New York, 1982).
25. J. SPANOUDAKIS and R. J. YOUNG, *J. Mater. Sci.* **19** (1984) 473; *ibid.* **19** (1984) 487.
26. A. C. MOLONEY, H. H. KAUSCH and H. R. STIEGER, *ibid.* **18** (1983) 208.
27. S. SAHU and L. J. BROUTMAN, *Polym. Eng. Sci.* **12** (1972) 91.
28. L. J. BROUTMAN and S. SHAU, *Mater. Sci. Eng.* **8** (1971) 98.
29. A. WAMBACH, K. TRACHTE and A. DIBENEDETTO, *J. Composite Materials* **2** (1968) 266.
30. F. F. LANGE, *Phil. Mag.* **22** (1970) 983.
31. F. F. LANGE and K. C. RADFORD, *J. Mater. Sci.* **6** (1971) 1197.
32. A. G. EVANS, *Phil. Mag.* **26** (1972) 1327.
33. R. J. YOUNG and P. W. R. BEAUMONT, *J. Mater. Sci.* **12** (1977) 684.
34. D. J. GREEN, P. S. NICHOLSON and J. D. EMBURY, *ibid.* **12** (1977) 987; *ibid.* **14** (1979) 1413; *ibid.* **14** (1979) 1657.
35. H. GAO and J. R. RICE, *Int. Journ. of Fracture* **33** (1987) 155.
36. G. PERRIN and J. R. RICE, *J. Mech. Phys. Solids* **42** (1994) 1047.
37. H. J. SUE and A. F. YEE, *J. Mater. Sci.* **28** (1993) 2975.
38. R. A. PEARSON and A. F. YEE, *ibid.* **21** (1986) 2475.
39. A. S. HOLIK, R. P. KAMBOUR, S. Y. HOBBS and D. G. FINK, *Microstruct. Sci.* **7** (1979) 367.
40. L. C. SAWYER and D. T. GRUBB, "Polymer Microscopy" (Chapman and Hall, New York, 1987).
41. R. A. PEARSON and A. F. YEE, *J. Mater. Sci.* **24** (1989) 2571.
42. C. J. SIMMONS and D. H. EL-BAYOUMI, "Experimental Techniques of Glass Science" (American Ceramic Society, Westerville, 1993).
43. O. ISHAI and L. J. COHEN, *Int J. Mech. Sci.* **9** (1967) 539.
44. A. S. ARGON, R. D. ANDREWS, J. A. GODRICK and W. WHITNEY, *J. Appl. Phys.* **39** (1968) 1899.
45. P. B. BOWDEN, *Phil. Mag.* **25** (1970) 455.
46. P. B. BOWDEN and S. RAHA, *ibid.* **25** (1970) 463.
47. J. LEE, Ph.D. thesis, The University of Michigan, 1998.
48. J. LEE and A. F. YEE, to be published.
49. H. H. KAUSCH, "Polymer Fracture" (Springer-Verlag, Berlin, 1987).
50. J. N. GOODIER, *J. Appl. Mech.* **55:A39** (1933) 39.
51. T. W. CLYNE and P. J. WITHERS, "An Introduction to Metal Matrix Composites" (Cambridge University, New York, 1993) p. 166.
52. C. H. WANG, *Engineering Fracture Mechanics* **56** (1997) 77.
53. T. S. CHOW and J. C. WILSON, *J. Polym. Sci. B* **16** (1978) 967.
54. H. WANG, S. LI, H. ZHOU, T. YU and X. JIN, *Polym. Eng. Sci.* **32** (1992) 678.
55. H. WANG, S. LI and T. YU, *ibid.* **33** (1993) 474.
56. A. KUSKE and G. ROBERTSON, "Photoelastic Stress Analysis" (John Wiley & Sons, 1974).
57. J. W. DALLY and W. F. RILEY, "Experimental Stress Analysis" (McGraw-Hill, New York, 1965).
58. C. B. BUCKNALL, "Toughened Plastics" (Applied Science, London, 1977).
59. L. S. SIGL, P. A. MATAGA, B. J. DALGLEISH, R. M. MCMEEKING and A. G. EVANS, *Acta Metall.* **36** (1988) 945.
60. R. A. PEARSON and A. F. YEE, *J. Mater. Sci.* **26** (1991) 3828.

Received 1 March
and accepted 22 May 2000